FULL PAPER

Dalton
www.rsc.org/dalton

Structural trends in copper(II) bis(thiosemicarbazone) radiopharmaceuticals †

Philip J. Blower,*[a] Thomas C. Castle,[a] Andrew R. Cowley,[b] Jonathan R. Dilworth,*[b] Paul S. Donnelly,[b] Elena Labisbal,[b] Frank E. Sowrey,[a] Simon J. Teat[c] and Michael J. Went[a]

[a] *School of Physical Sciences and Department of Biosciences, University of Kent, Canterbury, Kent, UK CT2 7NJ. E-mail: p.j.blower@kent.ac.uk*

[b] *Inorganic Chemistry Laboratory, University of Oxford, South Parks Road, Oxford, UK OX1 3QR*

[c] *CCLRC Daresbury Laboratory, Daresbury, Warrington, UK WA4 4AD*

Received 1st July 2003, Accepted 16th September 2003
First published as an Advance Article on the web 30th September 2003

Redox-related changes in biological properties of copper bis(thiosemicarbazone) radiopharmaceuticals are induced by backbone alkylation. To determine whether these changes are mediated by changes in core structural parameters, eight X-ray structures of variously alkylated complexes were determined. The complexes include the hypoxia tracer diacetylbis(4-methyl-3-thiosemicarbazonato)copper(II) (CuATSM). The structures of the nickel analogue NiATSM and the corresponding free ligand $ATSMH_2$ were also included. Distortions from planarity were slight and only present when there were significant intermolecular interactions (mainly pairs of N–H–N and N–H–S hydrogen bonds). These give rise to cross-linked flat or helical ribbons of complexes. Alkylation at the terminal nitrogen atoms interrupts hydrogen bonding, allowing complexes to become planar, but does not otherwise affect the coordination sphere. Alkylation at the backbone carbon atoms increases the backbone C–C bond length, allowing the metal to fit better into the ligand cavity with shorter Cu–S bonds.

Introduction

Copper bis(thiosemicarbazone) complexes[1,2] have been the focus of investigation as metallodrugs for various medical applications for over thirty years. These applications include use as anti-cancer drugs,[3] superoxide dismutase-like radical scavengers,[4] and positron emission tomography (PET) agents for imaging tissue perfusion[5] and more recently, tissue hypoxia.[6,7] The bis(thiosemicarbazone) ligands have also been used in the design of bifunctional chelators for labelling biomolecules with copper radioisotopes for PET.[8] The various biological properties required of the complexes for these different uses are obtained by virtue of the remarkable sensitivity of the electronic and redox properties of the complexes to the number and position of alkyl groups attached to the ligands. The most detailed studies of these structure–activity relationships have been carried out in connection with the hypoxia imaging application.[6,9–11] These studies have correlated hypoxic cell selectivity with reduction potential, electronic structure (as studied by density functional methods and spectroscopy) and chemical behaviour. It was found that all of these properties were extraordinarily sensitive to the number of alkyl groups attached to the diimine backbone of the ligand, but much less sensitive to the number of alkyl groups at the amino-terminal positions.

Since these relatively superficial modifications induce remarkable changes in redox and biological properties, it is natural to enquire whether they might significantly affect the core structural parameters of the complexes, and if so, whether this might be related to the biological behaviour (over and above the expected changes in lipophilicity). In this paper we report the X-ray crystal structures of eight copper bisthiosemicarbazone complexes with different alkylation patterns, as well as a nickel analogue and the corresponding free ligand for comparison. We discuss structural variations as a function of alkylation at the diimine backbone and at the amino-terminus (see Fig. 1 for ligand structures).

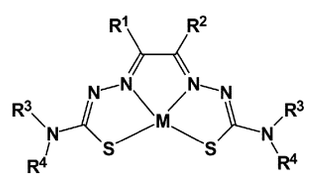

		R^1	R^2	R^3	R^4
1	CuGTS	H	H	H	H
2	CuGTSM	H	H	CH_3	H
3	CuGTSE	H	H	C_2H_5	H
4	CuPTS	CH_3	H	H	H
5	CuCTS	CH_3	C_2H_5	H	H
6	CuATSM	CH_3	CH_3	CH_3	H
7	CuDTS	C_2H_5	C_2H_5	H	H
8	CuATSM2	CH_3	CH_3	CH_3	CH_3
9	NiATSM	CH_3	CH_3	CH_3	H
10	$ATSMH_2$	CH_3	CH_3	CH_3	H

Fig. 1 Structures and abbreviations for compounds structurally characterised in this work.

Experimental

Complexes were synthesised as previously described except as indicated below. Analytical and spectroscopic properties were consistent with those previously reported.[6,12]

Diacetylbis(4-methyl-3-thiosemicarbazonato)nickel(II), 9

This complex, previously reported by Jones and McCleverty,[2] was obtained in crystalline form by electrochemical oxidation of nickel metal in an acetonitrile solution of $ATSMH_2$ **10** (0.024 g, 0.09 mmol) in the presence of tetrabutylammonium

† Electronic supplementary information (ESI) available: Fig. A: Comparison of average crystallographic, "template" and density functional "optimised" CuATSM (**6**) bond lengths. Fig. B: Paired N–H ··· N and N–H ··· S hydrogen bonding networks in complexes without terminal alkyl groups. Fig. C: Networks of Cu ··· S and N–H ··· S hydrogen bonds in complexes with monoalkylated terminal nitrogen atoms. Fig. D: Planar array of non-hydrogen bonded molecules in the crystal of **8**. Table A: Displacement (Å) of atoms from least squares planes. Table B: Torsional angles. See http://www.rsc.org/suppdata/dt/b3/b307499d/

DOI: 10.1039/b307499d

tetrafluoroborate (10 mg). The cell was a tall-form beaker (100 mL) containing a platinum wire cathode and a nickel foil anode. The initial voltage was 15.8 V with an intensity of 4 mA for 30 min and an electrochemical efficiency of 0.48 mol F^{-1}. Hydrogen was evolved at the cathode. These results are consistent with the following half-cell reactions: cathode: $ATSMH_2 + 2e^- \longrightarrow H_2 + ATSM^{2-}$; anode: $Ni + ATSM^{2-} \longrightarrow NiATSM + 2e^-$. Crystals of **9** were grown by slow evaporation from the electrolysed MeCN solution.

Crystals of **1**, **4** and **5** were grown by slow diffusion of water into dmso solutions of the complexes. Crystals of **2** were grown by slow diffusion of a solution of $GTSMH_2$ in dmso–ethanol into an ethanol solution of $Cu(en)_2Cl_2$ layered above it.[13] Crystals of **6a** and **7** were grown by slow diffusion of ethanol into dmso solutions of the complexes. Crystals of **8** were grown by slow diffusion of light petroleum (bp 40–60 °C) into a thf solution of the complex. Crystals of **6b** were prepared by allowing a solution of $[Cu(ATSMH_2)_2](PF_6)_2 \cdot 4dmf$[14] to stand in air. A large single crystal was cut to suitable dimensions. Crystals of **6c** were grown by slow evaporation from CH_2Cl_2 solution. Crystals of **10** were grown from a solution of the ligand in dmso. Large crystals appeared on standing over several days. The crystal data and X-ray diffraction data collection, structure solution and refinement methods for all complexes are summarised in Table 1.

For compounds **1**, **2**, **4**, **5**, **6a**, **7** and **8**, a single crystal was mounted on a glass fibre using perfluoropolyether oil and cooled rapidly to 150 K on an Oxford Cryosystems Cryostream[15] low-temperature unit. X-Ray diffraction data were measured, using silicon 111 monochromator and a Bruker SMART 1K CCD area detector diffractometer at station 9.8[16] of the SRS at Daresbury Laboratory. A multi-scan absorption correction was applied. The structures of all seven compounds were solved by direct methods using SHELXS-97[17a] and full-matrix least squares refinement on F^2 were undertaken using SHELXL97.[17b] All non-hydrogen atoms were refined anisotropically. For compound **5** displacement parameter restraints were used. All hydrogen atoms were either found in the difference map or placed geometrically and then refined using a riding model.

For compounds **3**, **6b**, **6c**, **9** and **10** a single crystal was mounted and cooled as above. X-Ray diffraction data were collected, using graphite monochromated Mo-Kα radiation, λ = 0.71073 Å, on an Enraf-Nonius Kappa CCD diffractometer. A semi-empirical absorption correction determined from equivalent reflections was applied. Intensity data were processed using the DENZO-SMN package.[18] The structures of all five compounds were solved by direct methods using the program SIR92.[19] Full matrix least squares refinement on F was undertaken using the CRYSTALS program suite.[20] Coordinates and anisotropic thermal parameters of all non-hydrogen atoms were refined. Hydrogen atoms were found in the difference Fourier map or placed geometrically and a common isotropic thermal parameter subsequently refined. A three-term Chebychev polynomial weighting scheme was applied.

Since we have studied a series of related complexes, comparisons between them can be statistically analysed to identify trends. Thus, the conventional "3σ" rule (where σ is the crystallographic estimated standard deviation in an individual structural parameter) for identifying significant differences in pairs of structural parameters is overridden by statistical analysis across the series. The statistical significance of differences in structural parameters caused by adding two alkyl groups to the diimine backbone was tested using the Mann Whitney U test. As there is only one complex with a single backbone alkyl group (CuPTS) and the structure of this was disordered, this complex was excluded from the statistical analysis. Three separate structure determinations for complex **6** were included in the statistical analysis, each using crystals grown under different conditions.

CCDC reference numbers 213898–213908 and 219684.

See http://www.rsc.org/suppdata/dt/b3/b307499d/ for crystallographic data in CIF or other electronic format.

Results and discussion

Bond lengths for all complexes are listed in Table 2, and bond angles for all complexes are listed in Table 3. Views of the molecular structures of complexes without alkyl groups in the diimine backbone are shown in Fig. 2 (exemplified by CuGTSM **2**, CuGTSE **3** only). Views of the structures with two backbone alkyl groups (exemplified by CuATSM **6a**, CuDTS **7**, CuATSM2 **8** and NiATSM **9**) are shown in Fig. 3. The structure of uncomplexed $ATSMH_2$ **10** is shown in Fig. 4. Together, these examples are sufficient to show both the main structural features and the atom labelling scheme used consistently across all structures to allow comparison. All complexes were close to the expected planar structure with three five-membered chelate rings, as observed for other examples of this type of complex.[13,22–27] The free ligand $ATSMH_2$ (**10**) was also close to planar, with a *trans*-configuration about the diimine backbone. Both *cis*[28,29] and *trans*[27,30,31] configurations have previously been observed in related molecules.

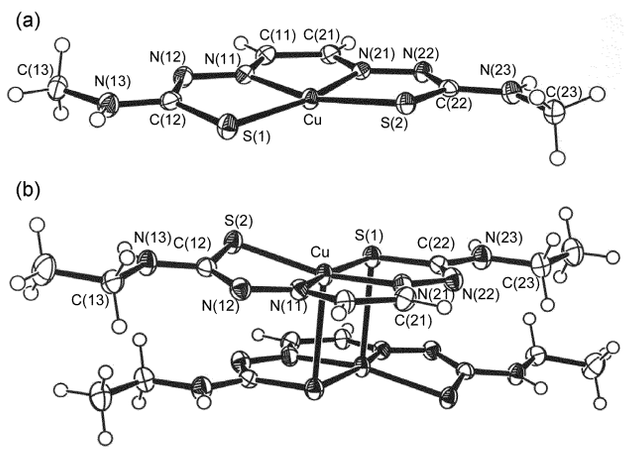

Fig. 2 ORTEP[21] views of the molecular structures CuGTSM **2** (upper) and CuGTSE **3** (lower), as examples of complexes with no backbone alkyl groups, showing atom labelling scheme.

Metal–ligand fit

The overall impression from bond angles around the copper atoms is of a ligand cavity too small to accommodate the Cu^{2+} ion ideally. The N–Cu–N bond angles are only 80° and the sulfur ends of the ligand arms are pushed outwards well beyond the natural position that would be adopted by the planar ligand with 120° bond angles. For comparison, the Ni^{2+} ion complexes with ATSM (**9**) and related ligands[23,24,27] show a much better fit. As a result of the smaller ionic radius of nickel (giving M–N and M–S distances of 1.86 and 2.16 Å, respectively in **9** compared to 1.97 and 2.25 Å for the copper complexes), all the angles at the nickel centre are significantly closer to the 90° angles preferred at the square planar metal centre. Thus, the average N–M–N angle in the copper complexes reported in this paper is 80.7° whereas for **9** and other nickel complexes[23,24,27] it is more than 83°. Similarly the S–M–S angles are 109.3° for Cu but only 102° for Ni, while the N–M–S angles are 84.9° for Cu and more than 87° for Ni. Although the ligand appears somewhat strained in the copper complexes, it has been shown that the ligands can open up even further to accommodate Cd^{2+} while maintaining an essentially planar structure.[32]

Bond lengths and resonance

The backbone C(11)–C(21) distances show the largest spread (S.D. = 0.012 Å) of all the intraligand bonds in the copper

Table 1 Crystal data

	1	2	3	4	5	6a[a]	6b[b]	6c	7	8	9[c]	10[d]
Formula	$C_4H_6CuN_6S_2$	$C_6H_{10}CuN_6S_2$	$C_8H_{14}CuN_6S_2$	$C_5H_7CuN_6S_2$	$C_7H_{12}CuN_6S_2$	$C_{10}H_{20}CuN_6OS_3$	$C_{11}H_{21}CuN_7OS_2$	$C_8H_{14}CuN_6S_2$	$C_8H_{14}CuN_6S_2$	$C_{10}H_{18}CuN_6S_2$	$C_{10}H_{17}N_7NiS_2$	$C_{12}H_{28}N_6O_2S_4$
M_r	265.81	293.86	321.90	278.83	307.89	400.04	395.00	321.90	321.91	349.96	358.12	416.64
λ/Å	0.6904[e]	0.6904[e]	0.71073	0.6904[e]	0.6904[e]	0.6872[e]	0.71073	0.71073	0.6872[e]	0.6904[e]	0.71073	0.71073
System	Monoclinic	Monoclinic	Triclinic	Monoclinic	Monoclinic	Monoclinic	Monoclinic	Monoclinic	Monoclinic	Triclinic	Monoclinic	Triclinic
Space group	$P2_1/c$	$P2_1/n$	$P\bar{1}$	$P2_1/c$	$C2/c$	$P2_1/c$	$P2_1/n$	$C2/c$	$P2/n$	$P\bar{1}$	$P2_1/c$	$P\bar{1}$
a/Å	6.7026(6)	4.0832(4)	8.8447(3)	5.5081(4)	17.878(7)	8.0485(13)	8.3300(2)	12.3084(4)	7.884(2)	7.3791(3)	7.2586(2)	9.4874(1)
b/Å	3.9436(3)	19.9969(19)	9.1298(3)	15.4057(10)	16.856(6)	14.086(2)	13.0822(3)	12.9874(5)	9.188(2)	8.5020(4)	16.9149(4)	11.2045(1)
c/Å	32.307(3)	12.7651(12)	9.5442(4)	11.6504(8)	7.978(3)	15.071(2)	16.2402(5)	8.2414(3)	17.962(5)	11.9417(5)	12.8679(3)	11.2427(1)
α/°	90	90	106.010(2)	90	90	90	90	90	90	104.281(2)	90	60.9079(3)
β/°	92.919(2)	98.607(2)	100.630(2)	102.193(2)	102.930(6)	97.864(3)	101.3738(9)	90.591	101.585	97.775(2)	105.8679(9)	87.3227(6)
γ/°	90	90	115.952(2)	90	90	90	90	90	90	90.630(2)	90	81.8540(5)
V/Å^3	852.84(12)	1030.55(17)	623.2	966.31(12)	2343.2(15)	1692.5(4)	1735.0	1317.4	1274.7(6)	718.59(5)	1519.7	1033.5
Z	4	4	2	4	8	4	4	4	4	2	4	2
D_c/g cm^{-3}	2.070	1.894	1.715	1.917	1.745	1.570	1.512	1.623	1.677	1.617	1.565	1.339
μ/mm^{-1}	3.007	2.498	2.074	2.659	2.202	1.667	1.511	1.962	2.028	1.806	1.552	0.477
F(000)	532	596	330.952	560	1256	828	821.937	661.905	660	362	745.995	444.919
Colour	Red	Red	Brown	Red	Yellow	Orange–red	Orange–brown	Red	Yellow	Red–orange	Brown	Colourless
Size/mm	0.60 × 0.02 × 0.01	0.30 × 0.02 × 0.01	0.06 × 0.08 × 0.10	0.14 × 0.08 × 0.04	0.12 × 0.06 × 0.01	0.30 × 0.03 × 0.02	0.14 × 0.22 × 0.35	0.08 × 0.10 × 0.16	0.04 × 0.02 × 0.005	0.12 × 0.06 × 0.02	0.30 × 0.30 × 0.30	0.16 × 0.24 × 0.26
θ collected/°	2.96–29.05	1.85–29.23	5.0–27.5	2.16–29.22	2.27–25.00	1.9–29.4	5.0–27.5	5.0–27.5	2.1–25.4	2.58–29.13	5.0–27.5	5.0–27.5
Index ranges, *hkl*	−9 to 9, −5 to 5, −44 to 42	−5 to 5, −27 to 26, −17 to 13	−11 to 11, −11 to 11, 0 to 12	−7 to 7, −21 to 21, −12 to 12	−21 to 21, −20 to 20, −9 to 9	−11 to 11, −19 to 19, −20 to 21	−10 to 10, 0 to 16, 0 to 21	−15 to 15, 0 to 16, 0 to 10	−9 to 9, −11 to 11, −20 to 22	−10 to 10, −11 to 8, −15 to 16	−9 to 9, 0 to 21, 0 to 16	−12 to 12, −12 to 14, 0 to 14
Refl. measured	7780	7252	9774	6518	9121	16313	12576	5344	6984	4988	11398	19519
Refl. unique	2328	2811	2802	2587	2248	4753	4137	1576	2566	3625	3567	4700
R_{int}	0.0320	0.0249	0.049	0.0232	0.0564	0.0452	0.022	0.031	0.0530	0.0068	0.027	0.025
Reflections obs., n ($I > n\sigma(I)$)	1946, 2	2229, 2	1835, 3	2165, 2	1694, 2	3976, 2	3321, 3	1259, 3	1817, 2	3055, 2	2968, 3	4097, 3
Max./min. transmission	0.95, 0.34	0.94, 0.61	0.88, 0.85	0.93, 0.68	0.98, 0.76	0.96, 0.62	0.81, 0.72	0.85, 0.82	0.96, 0.90	0.96, 0.83	0.63, 0.63	0.93, 0.89
Param. refined	118	138	197	139	147	196	200	100	156	178	249	302
R or $R1$ (obs. refl.)	$R1 = 0.0318$	$R1 = 0.0292$	$R = 0.0289$	$R1 = 0.0388$	$R1 = 0.0491$	$R1 = 0.0344$	$R = 0.0256$	$R = 0.0243$	$R1 = 0.0481$	$R1 = 0.0407$	$R = 0.0250$	$R = 0.0298$
wR or $wR2$ (all data)	$wR2 = 0.0751$ F^2	$wR2 = 0.0662$ F^2	$wR = 0.0321$ F	$wR2 = 0.0941$ F^2	$wR2 = 0.1192$ F^2	$wR2 = 0.0899$ F^2	$wR = 0.0285$ F	$wR = 0.0298$ F	$wR2 = 0.1222$ F^2	$wR2 = 0.1061$ F^2	$wR = 0.0285$ F	$wR = 0.0290$ F
GOF	0.976	0.937	1.0498	1.099	0.979	1.040	1.0364	0.9880	1.001	0.985	1.0336	1.1024
Residual peak, hole/e Å^{-3}	0.736, −0.648	0.524, −0.401	0.74, −0.34	0.628, −0.653	0.989, −0.970	0.46, −0.36	0.70, −0.32	0.61, −0.41	1.35, −0.77	0.629, −0.492	0.31, −0.27	0.69, −0.67

[a] Formula includes one molecule of dmso. [b] Formula includes one molecule of dmf. [c] Formula includes one molecule of MeCN. [d] Two independent molecules of the ligand, each situated on a crystallographic inversion centre, and formula includes two molecules of dmso. [e] Synchrotron radiation.

Table 2 Interatomic distances (Å) for all complexes **1**–**9** and ligand **10**, $ATSMH_2$

	1	**2**	**3**	**4**	**5**	**6a**[c]	**6b**[c]	**6c**[c]	**7**	**8**	**9**	**10** (mol. 1[b])	**10** (mol. 2[b])
C(11)–C(21)	1.453(3)	1.452(3)	1.458(4)	1.470(4)	1.480(7)	1.479(3)	1.479(2)	1.480(4)	1.480(6)	1.483(3)	1.470(3)	1.483(3)	1.479(4)
C(11)–C(1)				1.478(6)[a]	1.496(6)	1.490(3)	1.493(2)	1.498(3)	1.505(6)	1.487(3)	1.489(4)	1.499(3)	1.500(3)
C(21)–C(2)				1.486(6)[a]	1.517(7)	1.494(2)	1.493(2)	1.498(3)	1.501(6)	1.494(3)	1.491(3)	1.499(3)	1.500(3)
C(11)–N(11)	1.300(3)	1.307(3)	1.306(4)	1.298(3)	1.312(6)	1.298(2)	1.298(2)	1.296(3)	1.301(5)	1.299(3)	1.303(3)	1.294(2)	1.289(2)
C(21)–N(21)	1.296(3)	1.301(3)	1.296(4)	1.299(3)	1.295(6)	1.303(2)	1.296(2)	1.296(3)	1.301(5)	1.293(3)	1.305(2)	1.294(2)	1.289(2)
N(11)–N(12)	1.353(3)	1.363(2)	1.369(4)	1.365(3)	1.374(5)	1.373(2)	1.365(2)	1.369(3)	1.370(5)	1.369(3)	1.378(3)	1.377(2)	1.377(2)
N(21)–N(22)	1.370(3)	1.364(2)	1.363(3)	1.370(3)	1.373(5)	1.369(2)	1.369(2)	1.369(3)	1.377(5)	1.369(3)	1.375(3)	1.377(2)	1.377(2)
N(12)–C(12)	1.335(3)	1.337(3)	1.322(4)	1.336(3)	1.329(6)	1.323(2)	1.325(2)	1.325(3)	1.339(5)	1.330(3)	1.315(3)	1.369(2)	1.364(2)
N(22)–C(22)	1.326(3)	1.349(3)	1.331(4)	1.329(3)	1.331(6)	1.329(3)	1.324(2)	1.325(3)	1.324(5)	1.325(3)	1.319(3)	1.369(2)	1.364(2)
C(12)–S(1)	1.751(2)	1.756(2)	1.760(3)	1.753(3)	1.753(5)	1.7636(19)	1.7614(19)	1.759(2)	1.746(5)	1.772(2)	1.767(3)	1.6919(19)	1.685(2)
C(22)–S(2)	1.759(2)	1.755(2)	1.763(3)	1.756(3)	1.764(5)	1.7671(19)	1.7578(19)	1.759(2)	1.757(5)	1.762(2)	1.768(3)	1.6919(19)	1.685(2)
N(11)–M	1.9797(19)	1.9767(19)	1.965(3)	1.968(2)	1.969(4)	1.9592(16)	1.9602(15)	1.9583(17)	1.967(4)	1.965(2)	1.861(2)		
N(21)–M	1.9727(19)	1.9701(17)	1.977(3)	1.963(2)	1.975(4)	1.9654(16)	1.9619(14)	1.9583(17)	1.956(4)	1.9580(19)	1.855(2)		
S(1)–M	2.2506(6)	2.2435(6)	2.2735(8)	2.2340(8)	2.2350(14)	2.2474(6)	2.2363(5)	2.2453(5)	2.2274(14)	2.2408(6)	2.1546(6)		
S(2)–M	2.2710(6)	2.2812(6)	2.2505(8)	2.2431(8)	2.2458(15)	2.2473(6)	2.2464(5)	2.2453(5)	2.2424(13)	2.2511(7)	2.1598(7)		
C(12)–N(13)	1.332(3)	1.346(3)	1.348(4)	1.341(4)	1.329(6)	1.344(2)	1.344(2)	1.340(3)	1.332(6)	1.347(3)	1.339(3)	1.322(3)	1.331(3)
C(22)–N(23)	1.348(3)	1.337(3)	1.331(4)	1.348(4)	1.329(6)	1.341(2)	1.345(2)	1.340(3)	1.335(6)	1.356(3)	1.336(3)	1.322(3)	1.331(3)
C(1)–C(1A)					1.495(9)				1.511(8)				
C(2)–C(2A)									1.510(7)				
M–S inter-molecular	2.991	3.073	2.8045(9)										
N(13)–C(13)		1.452(3)	1.447(4)			1.462(3)	1.457(3)	1.444(3)		1.456(3)	1.449(3)	1.454(3)	1.451(3)
N(23)–C(23)		1.456(3)	1.468(4)			1.459(3)	1.450(3)	1.444(3)		1.462(3)	1.451(3)	1.454(3)	1.451(3)
N(13)–C(14)										1.456(3)			
N(23)–C(24)										1.449(3)			

[a] C(1) and C(2) in this structure are partially occupied sites representing only one carbon. [b] This structure has two independent molecules each situated on a crystallographic inversion centre. [c] Structure of **6** was determined three times from three different crystals grown under different conditions.

Table 3 Bond angles (°) for all complexes **1**–**9** and ligand **10**, $ATSMH_2$

	1	**2**	**3**	**4**[a]	**5**	**6a**	**6b**	**6c**	**7**	**8**	**9**	**10** (mol. 1[b])	**10** (mol. 2[b])
N(11)–C(11)–C(21)	115.2(2)	114.89(19)	114.2(3)	115.2(2)	114.2(4)	114.04(16)	114.13(15)	113.94(12)	114.0(4)	113.7(2)	112.5(2)	115.1(2)	114.2(2)
N(21)–C(21)–C(11)	115.3(2)	115.55(18)	115.6(3)	114.4(2)	114.5(4)	114.08(15)	114.03(15)	113.94(12)	113.7(4)	114.4(2)	112.9(2)	115.1(2)	114.2(2)
C(11)–N(11)–M	114.08(16)	114.22(15)	115.1(2)	114.31(18)	115.2(3)	115.83(13)	115.52(12)	115.78(15)	115.7(3)	115.51(16)	115.52(17)		
C(21)–N(21)–M	114.40(16)	114.24(14)	114.3(2)	114.89(18)	115.4(3)	115.38(13)	115.62(12)	115.78(15)	116.2(3)	115.61(16)	115.43(17)		
N(12)–N(11)–M	123.73(14)	124.40(13)	124.6(2)	123.60(16)	122.9(3)	123.67(11)	123.68(11)	123.46(13)	122.6(3)	123.30(15)	124.62(16)		
N(22)–N(21)–M	124.14(15)	124.14(13)	123.53(19)	123.49(17)	123.2(3)	123.68(12)	123.51(11)	123.46(13)	123.2(3)	123.45(15)	124.25(16)		
N(11)–N(12)–C(12)	111.68(18)	109.93(17)	109.9(3)	110.6(2)	111.3(4)	111.04(15)	110.80(14)	111.32(18)	111.0(4)	111.48(19)	109.6(2)	118.90(16)	117.33(17)
N(21)–N(22)–C(22)	111.12(18)	111.16(16)	110.7(2)	110.8(2)	111.3(4)	111.01(15)	111.02(14)	111.32(18)	111.3(4)	111.67(19)	110.0(2)	118.90(16)	117.33(17)
N(12)–C(12)–S(1)	125.01(17)	126.37(17)	127.5(2)	125.6(2)	125.6(4)	125.79(14)	125.94(13)	125.63(17)	125.7(4)	125.31(18)	124.12(18)	118.73(14)	119.12(15)
N(22)–C(22)–S(2)	125.53(17)	125.03(16)	125.3(2)	125.7(2)	125.5(4)	125.77(15)	126.04(14)	125.63(17)	125.5(4)	125.23(18)	124.13(19)	118.73(14)	119.12(15)
C(12)–S(1)–M	95.14(8)	94.65(7)	93.44(11)	94.83(9)	94.87(16)	94.39(6)	94.33(6)	94.44(8)	94.68(16)	94.46(8)	94.51(8)		
C(22)–S(2)–M	94.67(8)	94.48(7)	94.50(10)	94.49(10)	94.74(15)	94.34(7)	94.31(6)	94.44(8)	94.53(16)	94.53(8)	94.02(9)		
N(11)–M–N(21)	80.75(8)	81.02(7)	80.74(11)	81.20(9)	80.72(15)	80.62(6)	80.63(6)	80.55(10)	80.37(15)	80.68(8)	83.59(9)		
N(11)–M–S(1)	84.30(6)	84.58(5)	84.57(8)	84.88(7)	85.20(12)	85.07(5)	85.18(4)	85.14(5)	85.59(12)	85.44(6)	87.07(6)		
N(21)–M–S(2)	83.93(6)	84.01(5)	84.04(8)	84.89(7)	85.08(11)	85.12(5)	85.08(4)	85.14(5)	85.28(11)	85.02(6)	87.56(7)		
S(1)–M–S(2)	110.10(2)	110.24(2)	109.15(3)	109.53(3)	108.81(5)	109.23(2)	109.241(18)	109.21(3)	108.69(5)	108.77(2)	101.81(3)		
N(11)–M–S(2)	161.84(6)	162.35(5)	158.07(8)	165.11(7)	165.52(11)	165.52(5)	165.10(4)	165.61(5)	165.36(12)	165.55(6)	171.04(6)		
N(21)–M–S(1)	164.61(6)	165.59(5)	164.98(8)	164.46(7)	165.6(12)	165.65(5)	165.61(5)	165.61(5)	165.94(11)	165.99(6)	170.61(7)		
C(11)–C(1)–C(1A)					110.5(5)				111.8(4)				
C(21)–C(2)–C(2A)									113.2(4)				
C(11)–N(11)–N(12)	122.19(19)	121.38(19)	120.3(3)	122.1(2)	121.8(4)	120.49(16)	120.76(15)	120.76(17)	121.6(4)	121.2(2)	119.9(2)	116.85(16)	118.25(16)
C(21)–N(21)–N(22)	121.43(19)	121.52(17)	122.2(3)	121.6(2)	121.2(4)	120.91(16)	120.87(14)	120.76(17)	120.6(4)	120.8(2)	120.3(2)	116.85(16)	118.25(16)
C(1)–C(11)–C(21)				121.7(3)	122.3(4)	122.38(16)	122.51(15)	122.71(12)	123.8(4)	122.38(16)	123.7(2)	119.6(2)	119.5(2)
C(2)–C(21)–C(11)				122.4(3)	122.2(4)	121.90(17)	122.43(15)	122.71(12)	123.0(4)	121.90(17)	123.3(2)	119.6(2)	119.5(2)
C(1)–C(11)–N(11)				123.0(3)	123.3(4)	123.58(18)	123.35(16)	123.3(2)	122.2(4)	123.58(18)	123.7(2)	125.28(16)	126.24(17)
C(2)–C(21)–N(21)				123.0(3)	123.1(5)	124.02(18)	123.54(16)	123.3(2)	123.2(4)	124.02(18)	123.8(2)	125.28(16)	126.24(17)
N(12)–C(12)–N(13)	116.9(2)	117.29(19)	117.1(3)	117.2(2)	117.8(4)	117.34(17)	117.53(17)	117.5(2)	117.7(4)	116.5(2)	118.9(2)	117.36(17)	115.95(17)
N(22)–C(22)–N(23)	117.5(2)	114.8718)	118.5(3)	117.4(3)	117.1(4)	117.81(17)	116.80(17)	117.5(2)	117.6(4)	115.9(2)	119.4(2)	117.36(17)	115.95(17)
N(13)–C(12)–S(1)	118.07(17)	116.32(16)	115.4(2)	117.2(2)	116.6(3)	116.83(14)	116.53(14)	116.85(16)	116.6(3)	118.23(18)	116.9(2)	123.90(15)	119.12(15)
N(23)–C(22)–S(2)	117.00(18)	120.10(15)	116.1(2)	116.8(2)	117.4(3)	116.42(15)	117.16(14)	116.85(16)	116.8(3)	118.88(18)	116.5(4)	123.90(15)	119.12(15)
C(12)–N(13)–C(13)		123.50(19)	124.7(3)			122.00(16)	122.00(17)	123.0(2)		119.5(2)	122.3(2)	122.89(17)	124.15(18)
C(22)–N(23)–C(23)		125.65(18)	124.5(3)			122.18(18)	121.62(18)	123.0(2)		118.5(2)	123.6(3)	122.89(17)	124.15(18)

[a] C(1) and C(2) are partially occupied sites of one carbon. [b] This structure has two independent molecules per unit cell.

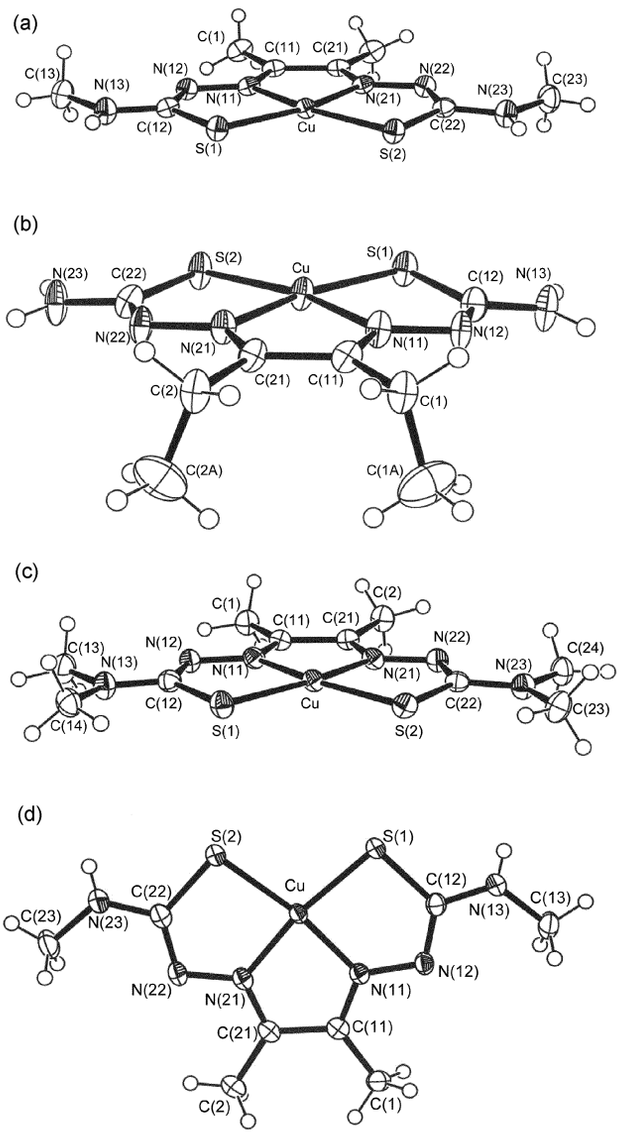

Fig. 3 ORTEP[21] views of the molecular structures of CuATSM **6c** (a), CuDTS **7** (b), and CuATSM2 **8** (c) and NiATSM **9** (d), as examples of complexes having two backbone alkyl groups, showing atom labelling scheme.

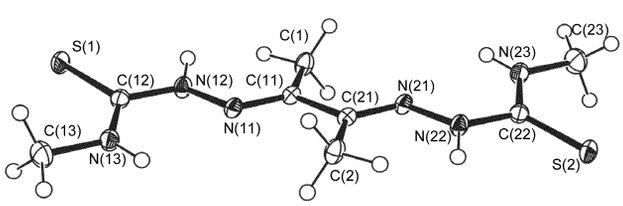

Fig. 4 View of structure of uncomplexed ligand $ATSMH_2$ **10**, showing atom labelling scheme.

complexes, ranging from 1.452 to 1.483 Å, consistent with a bond order greater than 1 but less than 1.5. Factors contributing to this spread are discussed below. The other corresponding intraligand bond distances are highly consistent across all the copper complexes (0.003 < S.D. < 0.008 Å). C(11)–N(11) distances range from 1.295 to 1.312 Å consistent with bond order greater than 1.5 but less than 2. These bonds are closer to a full double bond than any other bond in complex. N(11)–N(12) distances range from 1.353 to 1.377 Å consistent with bond order less than 1.5 but greater than 1. N(12)–C(12) distances range from 1.322 to 1.349 Å consistent with bond order less than that of C(11)–N(11), but still much greater than 1. C–S distances range from 1.746 to 1.772 Å consistent with bond order greater than 1 but less than 1.5. C(12)–N(13) (to terminal amines) range from 1.329 to 1.356 Å suggesting a bond order less than that of C(11)–N(11) and slightly less than that of N(12)–C(12) but still greater than 1. These data confirm that there is extensive conjugation within the ligand but that the resonance form depicted in Fig. 1 dominates. Comparison of the crystallographic bond lengths with fully optimised density functional-calculated bond lengths for CuATSM **6**[11] and with the template geometry used to calculate trends in orbital energies as a function of backbone alkylation[11] shows excellent agreement except that the template geometry significantly overestimates the C(12)–N(13) and C(22)–N(23) distances, and the optimised geometry slightly over-estimates copper–donor atom distances.

Effects of backbone C(11)–C(21) alkylation

The backbone alkylation pattern has been shown to affect redox potential,[2,6,9] UV spectra[33] and frontier orbital energies[11] and the hypoxic cell selectivity[6] more strongly than terminal alkylation. Therefore its effect on structural parameters is of particular interest. It was noted above that the C(11)–C(21) bond distance showed the largest spread. Examination of the trends (Fig. 5) in this parameter reveal a highly consistent and significant (p <0.025) increase in the backbone C(11)–C(21) bond length in complexes with two backbone alkyl groups (n = 2, average 1.478 Å) compared to those with none (n = 0, average 1.454 Å). The n = 1 data point in Fig. 5 includes CuPTS **4** as well as other previously published structures with n = 1 (CuKTS,[26] CuPg4DE[24] and CuPTSM[13]), and must be interpreted cautiously as **4** has disordered backbone alkyl groups. A previously published structure of the copper complex of the bis(thiosemicarbazone) derived from benzil, which has two backbone phenyl substituents,[22] was not included in the statistical analysis, but with a C–C distance of 1.49 Å is consistent with the observed trend. The structure of the free ligand **10**, combined with literature data, suggests that in the free ligands as well as in the complexes, alkylation of the C–C bond lengthens it, whether it has a *cis* or *trans* configuration. Thus, in four available structures of ligands with n = 1 (including two with R^1 = Ph,[29] one with R^1 = $CH(CH_3)OEt$,[26] and one with R^1 = (methylphthalimidomethyl),[28] the C–C bond lengths range from 1.447 to 1.463 Å, whereas in five ligands with n = 2 (including two with R^1 = Ph and R^2 = CH_3,[30] two with R^1 = R^2 = CH_3[27] including the present work, and one with R^1 = R^2 = Ph,[22]) it ranges from 1.458 to 1.49 Å. Unfortunately no crystallographic data are available for ligands with n = 0. The C(11)–C(21) bond length in **10** does not change significantly upon chelation of either copper or nickel. The lengthening of the C(11)–C(21) bond on alkylation was predicted by optimised density

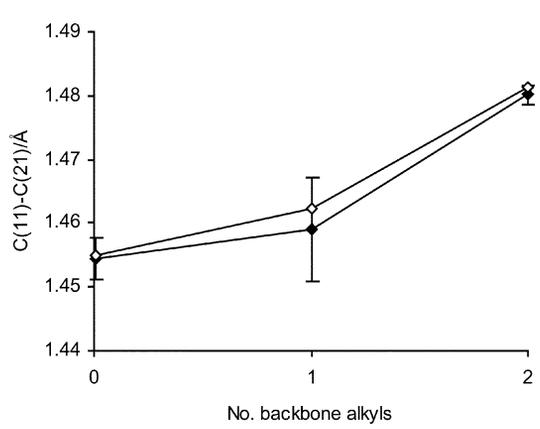

Fig. 5 Correlation of average crystallographically observed (filled symbols) and optimised BLYP density functional-calculated[11] (open symbols) C(11)–C(21) bond lengths with number of backbone alkyl groups. Crystallographic distances include copper complexes in Table 2 plus CuPTSM,[12] CuKTS[25] and CuPg4DE.[23] Error bars on crystallographic data points represent ± 1 standard deviation.

functional calculations[11] (Fig. 5) and the crystallographic data thus provide further experimental support for the validity of the calculations.

Backbone alkylation had a much smaller (but still significant at $p = 0.05$) lengthening effect on the N(11)–N(12) bonds from 1.36 to 1.37 Å. Effects of double alkylation on C(11)=N(11), and N(12)=C(12) distances in the ligand arms were not significant at the $p = 0.1$ level.

This observation of C(11)–C(21) bond lengthening raises the question of whether its causes are steric or electronic. Because the increase in bond length was predicted by density functional calculations[11] electronic causes were considered. Based on density functional calculations, the most obvious new orbital interaction one can envisage on alkylating C(11) and C(12) is a form of hyperconjugation between the LUMO (a very low-lying empty ligand-based π-orbital, see Fig. 6) and the alkyl C–H bonds. The calculations indeed suggested that alkylation of the backbone raised the energy of the ligand-based LUMO (Fig. 6) to a greater degree than other orbitals of similar energy, indicating a significant π-interaction. It is informative to compare this with the well-known case of hyperconjugation in ketones, where C–H bonds of α-carbon atoms overlap with the acceptor C–O π* orbital. This orbital is C–O antibonding, so that hyperconjugation lengthens the C–O bond. By contrast, in our copper complexes the calculated LUMO that can engage in a similar interaction with alkyl C–H bonds is strongly C(11)–C(21) π-*bonding*. Population of this orbital by hyperconjugation would therefore be expected to *shorten* the C(11)–C(21) bond – in conflict with experiment. Thus, although the calculations correctly predicted the increase in C–C bond length on alkylation, it is hard to reconcile the putative hyperconjugation effect with this increase.

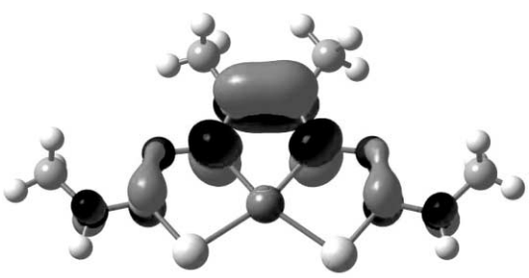

Fig. 6 Schematic representation of the ligand based LUMO calculated by dft.[11]

It is simpler, therefore, to assume that the bond lengthening is due to steric repulsion between the backbone alkyl groups. In support of this we note that second alkylation causes a much more substantial increase in bond length than the first. However, the steric argument remains tentative for a number of reasons. First, there is no obvious manifestation of such a repulsion in the bond angles about C(11) and C(21). In all the backbone-alkylated complexes except CuDTS, angles C(1)–C(11)–C(21) and C(2)–C(21)–C(11) (*ca.* 122°) are appreciably *less* than C(1)–C(11)–N(11) and C(2)–C(21)–N(21) (>123°). The disposition of ethyl groups in CuDTS is such that their methyl groups are oriented *syn* with respect to one another (Fig. 3), and perpendicular to the plane of the molecule. Similarly in CuCTS (not shown) the ethyl group has its methyl group oriented perpendicular to the plane of the complex. It is difficult to accept that this is the arrangement that would be preferred on steric grounds. Second, crystallographic data on the free ligands[22,26,27,29] and our data on $ATSMH_2$ (**10**) suggests that alkylation of the backbone lengthens the C–C bond in the uncomplexed ligands as well, even though the two alkyl groups in question are arrange *trans* to one another, relieving any steric pressure between them (Fig. 4).

What are the structural and chemical consequences of this change in C–C distance? The easiest way to visualise the structural changes accompanying the stretching of C(11)–C(21) resulting from alkylation is to view each arm of the ligand as more or less rigid, with a fixed point at the coordinated nitrogen (N(11), N(21)) about which the ligand arm pivots. Thus, as C(11)–C(21) stretches, each arm pivots about the coordinated nitrogen atoms so that the sulfur atoms are drawn inwards (Fig. 7), transmitting the changes to the metal coordination sphere. This view is consistent with the trends in angles expected from Fig. 7: when compared using a Mann Whitney U test, alkylation of C(11) and C(21) is accompanied by a small but significant decrease in C(11)–C(21)–N(21) ($p < 0.025$) and Cu–N(21)–N(22) ($p < 0.025$), and a decrease in S(1)–Cu–S(2) (although the latter does not reach significance at $p < 0.05$). Correspondingly there are significant increases in angles Cu–N(21)–C(21) ($p < 0.025$) and N(21)–Cu–S(2) (from average 84.24 to 85.16°, $p < 0.025$) (see Table 3). The remaining angles are not consistently or significantly affected. The changes are accompanied by significant ($p < 0.025$) shortening of the Cu–S bonds, as shown in Fig. 7, from an average of 2.262 to 2.243 Å. This too was predicted by density functional calculation.[11] Data for a complex with $R^1 = R^2 = Ph$ (mean Cu–S distance = 2.236 Å[22]) were not included in these averages but are consistent with the trends. The Cu–N bonds are shortened slightly on alkylation (as predicted by calculation), but the change is not statisticially significant. There is also a very small but statistically significant ($p < 0.025$) closing of the N–Cu–N angle from a mean of 80.83 to 80.60°. Overall, the trends in crystallographic results agree very well with those predicted by density functional calculations.[11] They suggest that addition of alkyl groups causes C(11)–C(21) lengthening which, although minor, in turn induces the ligand to embrace the metal more closely by allowing the sulfur arms to move inwards and accommodate the Cu ion more readily. Thus, upon alkylation of the diimine backbone, all of the structural parameters move slightly closer to those seen in the nickel complexes, in which, as noted above, there is a better metal–ligand "fit."

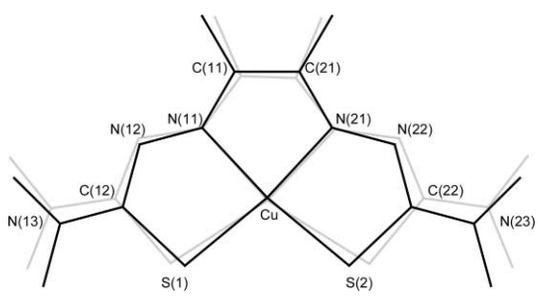

Fig. 7 Effect of C(11)–C(21) bond stretching on expansion of the ligand cavity by pivoting at coordinated nitrogen atoms. Grey lines: without backbone alkylation; bold lines: with alkylation at C(11) and C(21). Geometry changes are exaggerated for purposes of illustration.

Although any causative relationship between these structural parameters and biological function remains speculative, we note that categorisation of the complexes based on backbone C–C bond length coincides with the categorisation according to reduction potential, and in turn, with biological hypoxia-selectivity. Thus, the complexes with a long C–C bond have the lowest reduction potential (hardest to reduce) and the highest hypoxia selectivity, while those with a short C–C bond have the highest reduction potential and lowest hypoxia selectivity. The mechanical consequences of C–C bond length changes may contribute to the influence of alkylation in lowering the oxidation potential, since the better metal–ligand fit would be expected to raise the energy of the HOMO (which has principally M–L σ* character). It could also impact on the behaviour of the complexes upon reduction. If the LUMO is indeed a ligand based orbital with predominantly C(11)–C(21) π-bonding character (Fig. 6), as calculations suggest,[11] we should expect that when an electron is added to this orbital,

Table 4 Intermolecular contacts, hydrogen bonding, *etc.*

	Interaction	D–H/Å	H ··· A/Å	D ··· A/Å	D–H ··· A/°	Other/Å
1	N(13)–H(13A) ··· N(12A)	0.88	2.08	2.953(3)	174.7	
	N(13)–H(13B) ··· S(1B)	0.88	2.61	3.411(2)	151.0	
	N(23)–H(23A) ··· N(22C)	0.88	2.22	3.049(3)	157.9	
	Cu ··· S					2.991
2	N(13)–H ··· S(2A)	0.88	2.83	3.642(2)	154.1	
	N(23)–H ··· N(22B)	0.88	2.20	3.010(2)	152.0	
	Cu ··· S					3.073
3	Cu ··· S					2.8045(9)
	N(23)–H ··· S(2)	0.88	2.55	3.404(3)	167	
4	N(13)–H(13A) ··· N(12A)	0.88	2.18	3.057(3)	174.1	
	N(13)–H(13B) ··· S(2B)	0.88	2.71	3.580(2)	168.7	
	N(23)–H(23A) ··· N(22C)	0.88	2.15	3.025(4)	171.2	
	N(23)–H(23B) ··· S(1D)	0.88	2.84	3.531(3)	136.4	
5	N(13)–H(13A) ··· N(12A)	0.88	2.12	3.000(5)	178.7	
	N(23)–H(23A) ··· N(22B)	0.88	2.29	3.060(6)	145.8	
	N(23)–H(23B) ··· S(2C)	0.88	2.64	3.519(4)	173.6	
6a	N(13)–H(13) ··· O(1S)	0.88	2.07	2.945(2)	177	
	N(23)–H(23) ··· O(1SA)	0.88	2.22	3.072(2)	162	
6b	N(13)–H ··· O	0.79	2.20	2.979(2)	166	
	N(23)–H ··· O	0.81	2.26	3.023(2)	158	
6c	N(13)–H ··· S(1)	0.88	2.54	3.405(2)	168	
7	N(13)–H(13A) ··· N(12A)	0.88	2.13	3.007(6)	173	
	N(23)–H(23A) ··· N(22B)	0.88	2.23	3.034(5)	151	
	N(23)–H(23B) ··· S(2C)	0.88	2.6	3.482(4)	178	
8	None					
9	N(23)–H ··· S(1)	0.79	2.59	3.363	167	

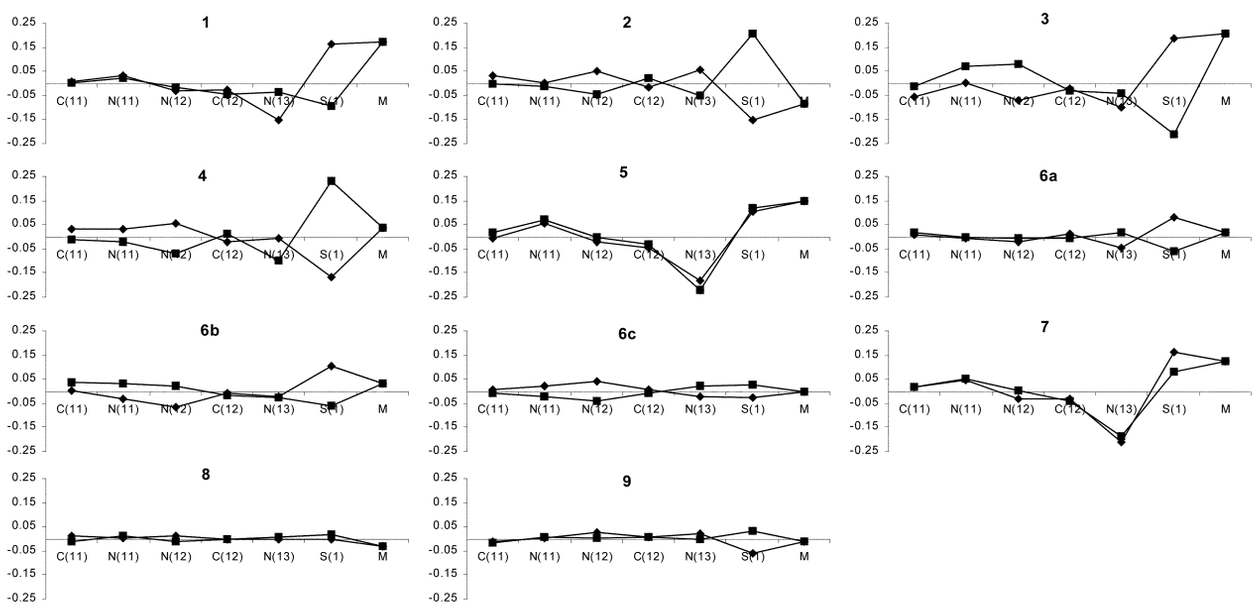

Fig. 8 Displacement (Å) of atoms from least squares plane defined by metal atom, S(1), S(2), C(11), C(21), C(12), C(22), N(11), N(21), N(12), N(22), N(13), N(23); ◆, S(1) arm; ■, S(2) arm.

there would be a shortening of the C(11)–C(21) bond, resulting in opening of the ligand embrace by pivoting at the coordinated nitrogens as in Fig. 7, thus weakening the Cu–S bonds and widening the S–Cu–S angle.

Effects of N-terminal alkylation

Effects of terminal alkylation on redox potential, electronic spectra and hypoxic cell selectivity are much less marked than those of backbone alkylation.[2,6,9,11] The structural effects of backbone and terminal alkylation parallel this trend: the clear-cut changes in bond lengths and angles (and reduction potential) in response to backbone alkylation are not apparent in response to terminal alkylation.

Planarity

The ease of deformation away from planarity could be connected with redox potential and other aspects of redox behaviour because distortions towards tetrahedral might favour reduction. Therefore it is pertinent to examine effects of alkylation on planarity and ligand rigidity. This can be addressed through least-squares displacement of ligand atoms from the mean plane of the complex. Fig. 8 shows displacement of ligand atoms from the least-squares plane for complexes **1**–**9**. It is noticable that the complexes closest to planar are **6c**, **8** and **9**, *i.e.* those in which intermolecular interactions (H-bonding or S–Cu contacts *etc.*, see below) are absent or precluded by alkylation of carbon (sterically blocking metal–ligand intermolecular contacts) or nitrogen (removing N–H bonds thus precluding H-bonding between complexes). This trend is reflected in the torsional angles as well (data not shown). This suggests that deviations from planarity observed here and in previously determined copper bis(thiosemicarbazone) structures are a consequence of external crystal packing forces and intermolecular interactions, and are not inherent in the molecular structure. In connection with steric interactions between

backbone alkyl groups, we note that any such interaction is insufficient to affect the torsional angles in the C(11)–C(21) bond: there is no consistent or significant variation and the N(11)–C(11)–C(21)–N(21) torsional angle is less than 2.4° in all cases.

Supramolecular architecture

It has been pointed out previously that the hydrogen-bonding groups in these complexes are well-equipped to form double hydrogen bonds with the nucleoside bases,[22] peptide bonds and other related biologically relevant molecules. In the crystal this capability gives rise to combinations of paired intermolecular hydrogen bonds N–H–N and N–H–S (Fig. 9) and intermolecular M–S interactions (*e.g.* **3** in Fig. 2) leading to interesting extended architectures. Pertinent intermolecular contact distances are listed in Table 4.

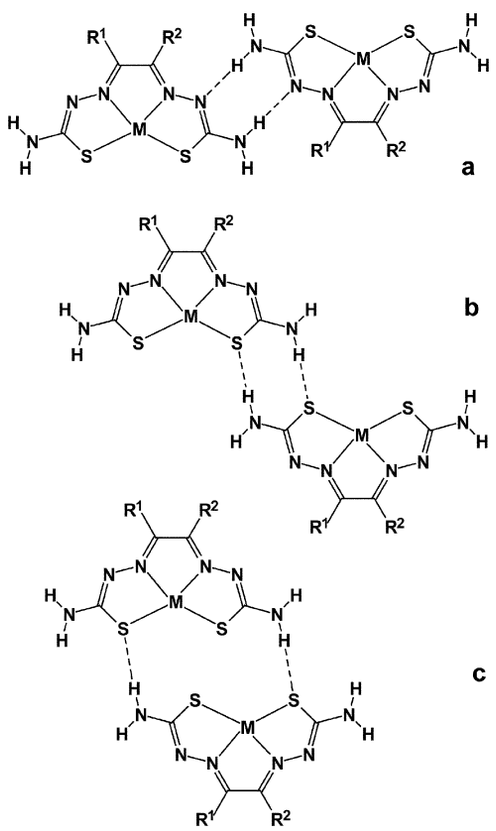

Fig. 9 Schematic illustration of NH–N and NH–S intermolecular bonding motifs present in the crystals.

Those complexes whose terminal nitrogen atoms are not alkylated (**1**, **4**, **5**, **7**) show the most extensive cross-linking. For example, **4**, **5** and **7** have flat (**4**, Fig. 10) or undulating (**5**, **7**) ribbons of complexes linked by paired mutually reinforcing N–H–N hydrogen bonds of the type shown in Fig. 9(a). These ribbons are cross-linked by paired, mutually reinforcing N–H–S hydrogen bonds of the type shown in Fig. 9(b) (**4**) or Fig. 9(c) (**5** and **7**, both of which share similar hydrogen-bonding patterns). In **1** (Fig. 10) one thiosemicarbazone arm is engaged in both N–H–S and N–H–N hydrogen bond simultaneously: the molecules are arranged in planar pairs linked by a pair of N–H–N hydrogen bonds, and each pair is linked to another by a pair of N–H–S hydrogen bonds, forming a roughly planar ribbon two molecules wide. Each ribbon is linked to others above and below the plane by unpaired hydrogen bonds through the other thiosemicarbazone arm.

Complexes with one alkyl group at the terminal nitrogen (**2**, **3**, **6**) also engage in hydrogen bonding *via* the remaining N–H bond, but without the extensive cross-linking between chains seen in **1**, **4**, **5** and **7**. Each dimer of **3** consists of two symmetry-related complexes linked by pairs of long intermolecular Cu–S bonds (Fig. 2). The dimers are linked into chains by pairs of reinforcing N(23)–H–S hydrogen bonds. Thus, each monomer is linked to two others, within the plane of the molecule by a pair of N–H–S hydrogen bonds and orthogonally to the plane by an intermolecular S(2)–Cu bond, to form a staircase-like structure. Complex **6c** (in which there is no solvent in the crystal) forms simple ribbons *via* flat zigzag chains of paired N–H–S hydrogen bonds running down the centre of the ribbon (Fig. 10) with the non-polar groups at the periphery, effectively preventing hydrogen bonding between ribbons. In **6a** and **6b**, crystallised from dmso or dmf, respectively, there is no direct

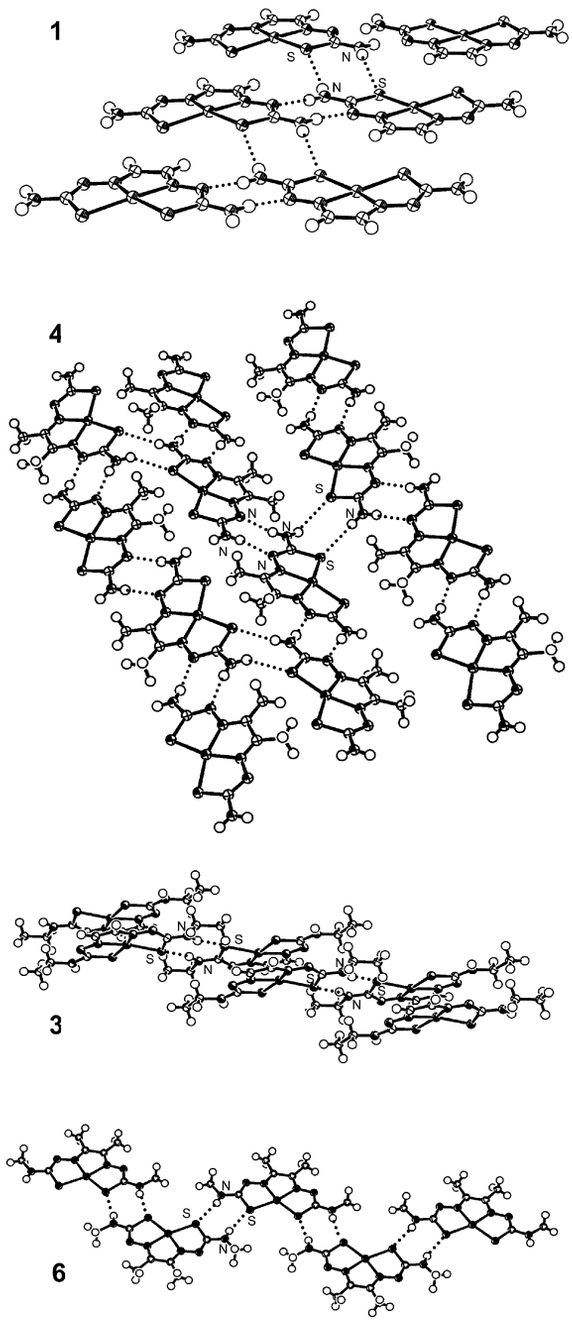

Fig. 10 Paired N–H–N and N–H–S hydrogen-bonding networks in complexes without terminal alkyl groups (**1** and **4**, top) and with monoalkylated terminal nitrogen atoms (**3** and **6c**, bottom). In **1**, molecules are linked into pairs by paired N–H–N hydrogen bonds, and the pairs are linked into ribbons by paired N–H–S hydrogen bonds. In **4**, molecules are linked into ribbons by paired N–H–N hydrogen bonds and the ribbons are cross-linked by paired N–H–S hydrogen bonds. In **3** staircase-like chains are formed by alternating paired Cu–S bonds and paired N–H–S hydrogen bonds. In **6c** simple flat ribbons are formed by zigzag chains of paired N–H–S hydrogen bonds.

hydrogen bonding between complexes. Instead the terminal N–H bonds form single hydrogen bonds with the solvent oxygen atom. In **9**, N(13) is not H-bonded, while N(23) takes part in intermolecular H-bonding with S(1) of another molecule to form chains linked through only one H bond, N(23)–H–S(1).

Complex **8** with two alkyl groups on each terminal nitrogen has no hydrogen-bonding capability. The alkyl groups also prevent close intermolecular intermolecular contact between copper and sulfur or nitrogen atoms and the crystal consists of stacks of the planar layers.

The issue of whether intermolecular axial interactions between potential Lewis bases and the copper centre are significant has been raised in connection with biological activity. The closest intermolecular Cu–S contacts in each of the present structures are listed in Table 4. Significant intermolecular contacts involving copper are seen only in complexes without alkylation in the backbone (CuGTS, GTSM, GTSE). This suggests that despite previous suggestions based on relatively limited data,[13,26] axial ligand bonding to copper is only a minor influence, easily overpowered by intermolecular steric hindrance from alkyl groups or by other crystal packing forces.

Summary and conclusions

The complexes are inherently planar, as predicted previously by computational methods. Any slight distortions from this are due only to intermolecular interactions, especially pairs of N–H–N and N–H–S hydrogen bonds. These give rise to supramolecular architectures involving cross-linked flat or helical ribbons of complexes, and may allow the complexes to interact with various biological molecules containing complementary hydrogen-bonding motifs (*e.g.* purines, pyrimidines and peptide bonds). Alkylation at the terminal nitrogen atoms interrupts intermolecular interactions allowing complexes to adopt idealised tetragonal planar geometry. Alkylation at the backbone carbon atoms increases the backbone C–C bond length. Although this was predicted by density functional calculations, and is also observed in the free ligands, the specific orbital interactions or steric interactions giving rise to it are not clearly defined. This C–C bond lengthening has consequences for the coordination sphere, allowing the metal to fit slightly better into the ligand cavity, which in turn may affect complex stability and redox potential.

Acknowledgements

We thank the EPSRC for grants supporting F. E. S. and P. S. D.

References

1 G. Bahr, *Z. Anorg. Allg. Chem.*, 1952, **268**, 351; G. Bahr, *Z. Anorg. Allg. Chem.*, 1953, **273**, 325; G. Bahr and E. Schleitzer, *Z. Anorg. Allg. Chem.*, 1955, **278**, 136.
2 C. J. Jones and J. A. McCleverty, *J. Chem. Soc. A*, 1970, 2829.
3 D. H. Petering, in *Carcinostatic copper complexes*, ed. H. Sigel, Marcel Dekker, New York, 1980; D. X. West, I. H. Hall, K. G. Rajendran and A. E. Liberta, *Anticancer Drugs*, 1993, **4**, 231.
4 K. Wada, Y. Fujibayashi, N. Tajima and A. Yokoyama, *Biol. Pharm. Bull.*, 1994, **17**, 701.
5 M. A. Green, C. J. Mathias, M. J. Welch, A. H. McGuire, D. Perry, F. Fernandez-Rubio, J. S. Perlmutter, M. E. Raichle and S. R. Bergmann, *J. Nucl. Med.*, 1990, **31**, 1989.
6 J. L. J. Dearling, J. S. Lewis, G. E. D. Mullen, M. J. Welch and P. J. Blower, *J. Biol. Inorg. Chem.*, 2002, **7**, 249.
7 Y. Fujibayashi, H. Taniuchi, Y. Yonekura, H. Ohtani, J. Konishi and A. Yokoyama, *J. Nucl. Med.*, 1997, **38**, 1155; J. S. Lewis, D. W. McCarthy, T. J. McCarthy, Y. Fujibayashi and M. J. Welch, *J. Nucl. Med.*, 1999, **40**, 177; A. Obata, E. Yoshimi, A. Waki, J. S. Lewis, N. Oyama, M. J. Welch, H. Saji, Y. Yonekura and Y. Fujibayashi, *Annal. Nucl. Med.*, 2001, **15**, 499; J. S. Lewis and M. J. Welch, *Quart. J. Nucl. Med.*, 2001, **45**, 183; J. S. Lewis, T. L. Sharp, R. Laforest, Y. Fujibayashi and M. J. Welch, *J. Nucl. Med.*, 2001, **42**, 655; J. S. Lewis, R. Laforest, T. L. Buettner, S. K. Song, Y. Fujibayashi, J. M. Connett and M. J. Welch, *Proc. Natl. Acad. Sci. USA*, 2001, **98**, 1206.
8 K. Matsumoto, Y. Fujibayashi, K. Arano, A. Wada and A. Yokoyama, *Nucl. Med. Biol.*, 1992, **19**, 33; D. W. McPherson, G. Umbricht and F. F. J. Knapp, *J. Labelled Cpd. Radiopharm.*, 1990, **28**, 877; R. S. Wu, *Eur. Pat*., EP 0 306 168 A1, 1989.
9 J. L. J. Dearling, J. S. Lewis, D. W. McCarthy, M. J. Welch and P. J. Blower, *Chem. Commun.*, 1998, 2531.
10 J. L. J. Dearling, J. S. Lewis, G. E. D. Mullen, M. T. Rae, J. Zweit and P. J. Blower, *Eur. J. Nucl. Med.*, 1998, **25**, 788.
11 R. I. Maurer, P. J. Blower, J. R. Dilworth, C. A. Reynolds, Y. F. Zheng and G. E. D. Mullen, *J. Med. Chem.*, 2002, **45**, 1420.
12 H. Beraldo, L. P. Boyd and D. X. West, *Transition Met. Chem.*, 1998, **23**, 67.
13 E. John, P. E. Fanwick, A. T. Mckenzie, J. G. Stowell and M. A. Green, *Nucl. Med. Biol.*, 1989, **16**, 791.
14 A. R. Cowley, J. R. Dilworth, P. S. Donnelly, E. Labisbal and A. Sousa, *J. Am. Chem. Soc.*, 2002, **124**, 5270.
15 J. Cosier and A. M. Glazer, *J. Appl. Crystallogr.*, 1986, **19**, 105.
16 R. J. Cernik, W. Clegg, C. R. A. Catlow, G. Bushnell-Wye, J. V. Flaherty, G. N. Greaves, M. Hamichi, I. Burrows, D. J. Taylor and S. J. Teat, *J Synchrotron Radiat.*, 1997, **4**, 279.
17 (*a*) G. M. Sheldrick, SHELXS-97, Program for solution of crystal structures, University of Göttingen, Germany, 1997; (*b*) G. M. Sheldrick, SHELXL-97, Program for refinement of crystal structures, University of Göttingen, Germany, 1997.
18 Z. Otwinowski and W. Minor, *Methods Enzomol.*, 1997, **276**, 276.
19 D. J. Watkin, C. K. Prout, J. R. Carruthers, P. W. Betteridge and R. I. Cooper, in CRYSTALS, Oxford, 2001.
20 A. Altomare, G. Cascarano, G. Giovazzo, A. Guadliardi, M. C. Burla, G. Polidori and M. Camalli, *J. Appl. Crystallogr.*, 1994, **27**, 435.
21 M. N. Burnett and C. K. Johnson, ORTEP-III: Oak Ridge Thermal Ellipsoid Plot Program for Crystal Structure Illustrations, Report ORNL-6895, Oak Ridge National Laboratory, Oak Ridge, TN, USA, 1996.
22 G. W. Bushnell and A. Y. Tsang, *Can. J. Chem.*, 1979, **57**, 603.
23 L. J. Ackerman, P. E. Fanwick, M. A. Green, E. John, W. E. Running, J. K. Swearingen, J. W. Webb and D. X. West, *Polyhedron*, 1999, **18**, 2759.
24 A. Castineiras, E. Bermejo, D. X. West, A. K. El-Sawaf and J. K. Swearingen, *Polyhedron*, 1998, **17**, 2751.
25 M. R. Taylor, E. J. Gabe, J. P. Glusker, J. A. Minkin and A. L. Patterson, *J. Am. Chem. Soc.*, 1966, **88**, 1845.
26 M. R. Taylor, J. P. Glusker, E. J. Gabe and J. A. Minkin, *Bioinorg. Chem.*, 1974, **3**, 189.
27 D. X. West, J. S. Ives, G. A. Bain, A. E. Liberta, J. Valdes-Martinez, K. H. Ebert and S. Hernandez-Ortega, *Polyhedron*, 1997, **16**, 1895.
28 L. Xiu-Yun, Z. Qi-Tai, S. Fu-Ling, W. Lin and Z. Zhi-Zhong, *Chin. Sci. Bull.*, 1989, **34**, 1217.
29 A. Castineiras, E. Bermejo, L. J. Ackerman, H. Beraldo and D. X. West, *J. Mol. Struct.*, 1999, **477**, 1.
30 A. Castineiras, E. Bermejo, L. J. Ackerman, H. Beraldo, J. Valdes-Martinez, S. Hernandez-Ortega and D. X. West, *J. Mol. Struct.*, 1999, **510**, 157.
31 E. J. Gabe, M. R. Taylor, J. P. Glusker, J. A. Minkin and A. L. Patterson, *Acta Crystallogr., Sect. B*, 1969, **25**, 1620.
32 E. Lopez-Torres, M. A. Medniola, J. Rodriguez-Procopio, M. T. Sevilla, E. Colacio, J. M. Moreno and I. Sobrados, *Inorg. Chim. Acta*, 2001, **323**, 130.
33 T. C. Castle, R. I. Maurer, F. E. Sowrey, M. J. Went, C. A. Reynolds, E. J. L. McInnes and P. J. Blower, *J. Am. Chem. Soc.*, 2003, **125**, 10040.